Tellus (1989), *41A*, 132–147

The effect of parameterized ice microphysics on the simulation of vortex circulation with a mesoscale hydrostatic model

By DA-LIN ZHANG, *National Center for Atmospheric Research*, Boulder, CO 80307-3000, USA

(Manuscript received 30 November 1987; in final form 26 April 1988)

ABSTRACT

It has been proposed that ice microphysics, particularly the melting effect, can play an important rôle in the generation of mesoscale structure and evolution of convective weather systems and associated stratiform rainfall. In this paper, parameterized cloud ice and snow crystals are incorporated into an explicit (grid-resolved) convective scheme as prognostic variables and tested using an observed mesovortex on a grid resolution of 25 km.

With the inclusion of ice microphysics parameterization, the resolvable-scale precipitation begins to develop nearly 1 h earlier and undergoes a more rapid acceleration. Meanwhile, the resulting maximum upward motion and locally accumulated rainfall are significantly larger than that without ice microphysics. However, the model produced a relatively weak mesovortex circulation with the maximum cyclonic vorticity located more than 50 mb higher when the ice microphysics is incorporated. It is found that the freezing and sublimation provide a positive forcing for the rapid development of the mid-tropospheric warm-core vortex circulation, while the melting tends to destroy the concentration of cyclonic vorticity in the lower levels. In particular, intercomparisons among all sensitivity experiments so far performed reveal that the melting effect can be of equal importance to those of the hydrostatic water loading and evaporative cooling in retarding the development of the CISK-like instability and in reducing the intensity of the mesovortex. The results indicate that the vertical distribution of diabatic heating may be more important than the total heating in determining the strength of mesovortices, when the melting effect is considered.

1. Introduction

It has been recognized for more than 5 decades that ice particles play an important rôle in the formation of precipitation (Bergeron, 1935). This recognition formed the experimental basis for dynamic cloud seeding in which massive artificial ice nucleation in updraft regions increases buoyancy through additional latent heat release of fusion and sublimation (Simpson et al., 1965). In addition, many numerical simulations of individual clouds show that incorporation of ice-phase microphysics tends to produce more realistic structure and evolution of convective storms than that without ice-phase microphysics (e.g., Orville and Kopp, 1977; Cotton et al., 1982; Lin et al., 1983).

However, the significance of ice-phase microphysics in the generation of mesoscale structure and evolution did not become evident until Zipser (1969; 1977) and others noted characteristic "diamond-shaped" thermal profiles often present in the trailing stratiform region of tropical squall lines. Those profiles exhibit a gradual separation of temperature and dew point curves below the 0°C isotherm and then a merging of the curves on approaching the surface. Such a thermal structure suggests the existence of mesoscale unsaturated downdrafts that may partly result from the melting and

[1] The National Center for Atmospheric Research (NCAR) is funded by the National Science Foundation.

evaporation of frozen particles. The "diamond-shaped" soundings have also been found in many mesoscale convective systems (MCSs) in midlatitudes (Ogura and Liou, 1980; Johnson, 1986; Leary and Rappaport, 1987). In particular, the 0°C isotherm, which is often observed as a "bright band" in radar echoes, has been conceptually regarded as the demarcation between mesoscale updrafts associated with predominant stratiform (anvil) clouds and mesoscale downdrafts beneath for tropical cloud clusters (see Houze, 1977). A recent Doppler radar study by Chong et al. (1987) appears to support such a conceptual flow structure. Furthermore, Leary and Houze (1979) investigated five cases of tropical anvil clouds and found that cooling rates due to melting of ice particles were conparable to that by evaporation of raindrops within 1-km layer immediately below the melting level. This further suggests that melting can be an important factor for the initiation or maintenance of mesoscale downdrafts. In fact, numerical sensitivity studies by Willoughby et al. (1984) and Lord et al. (1984) confirm that the widespread cooling by melting of frozen particles can generate a preferred region for the development of mesoscale downdrafts. Srivastava (1987) also showed that the melting of ice particles increases the intensity of downdrafts.

Recently, the importance of ice microphysics has been further emphasized. Churchill and Houze (1984) observed during the Winter Monsoon Experiments (WMONEX) that the stratiform region of tropical cloud clusters were largely composed of ice particles and responsible for more than 45% of the total precipitation. Based upon the fact that within the mid- to upper-troposphere there often exists a front to rear relative flow accompanying MCSs and associated stratiform clouds, Smull and Houze (1987) proposed a hypothesis that the fallout of rearwardly advected ice particles from the leading convective line can be responsible for most of precipitation in the trailing stratiform region. Later, with a two-dimensional diagnostic model, Rutledge and Houze (1987) obtained some plausible results for the validation of the Smull–Houze hypothesis, although their results appear to be sensitive to the magnitude of the front to rear flow and the vertical distribution of hydrometeors. The trailing stratiform region has also been found to be a favorable location for the development of mesovortices—an important component of MCSs and many recent studies have shown the presence of large amount of widespread low- to mid-level stratiform precipitation associated with those vortex systems (Churchill and Houze, 1984; Rockwood et al., 1984; Smull and Houze, 1987; Zhang and Fritsch, 1987).

From the above brief review, it is apparent that explicit incorporation of ice microphysics into mesoscale can be very important not only for the reasonable prediction of resolvable-scale precipitation, but also for the realistic simulation of the mesoscale structure and evolution of convective weather systems. In particular, Zhang and Fritsch (1987) and Zhang et al. (1988) pointed out that as the grid size decreases to capably resolve mesoscale features, the grid-scale phase changes need to be described realistically, since it has been widely recognized that with such a grid spacing resolvable-scale updrafts and downdrafts become an integral part of MCSs and phase-change processes (Zipser, 1977; Houze, 1977; Ogura and Liou, 1980; Brown, 1979; Leary, 1980; Maddox, 1983). Furthermore, Molinari and Dudek (1986), Kalb (1987) and Zhang et al. (1988) found that mesoscale models are prone to the unrealistic development of the conditional instability of the second kind (or the CISK-like instability) when simulating mesovortices or when a model cyclone is falsely generated (so-called *numerical point storm*) as a result of unsatisfactory mechanisms to release local gravitational instability (also see Kasahara, 1961). (The CISK-like instability is referred to by Zhang et al. (1988) as an overenhanced positive feedback process on the resolvable scale among latent heat release, moisture convergence and the surface pressure fall.) Molinari and Dudek (1986) and Zhang et al. (1988) also illustrated that the incorporation of resolvable-scale evaporation and hydrostatic water loading helps stabilize the vertical atmospheric column, and thus retards the development of the CISK-like instability. Thus, it is desirable to include an additional retarding factor through melting of ice particles for the control of the CISK-like instability. Moreover, the rôles of ice-phase microphysics in mesoscale hydrostatic models have not been rigorously examined with real-data cases.

For the purpose of investigating the effect of parameterized ice microphysics on the simulation of MCSs, an observed mesovortex that developed in the 19–20 July 1977 Johnstown, Pennsylvania (USA) flood events is chosen for this study. The development of most mesovortices has been found to be strongly linked to the resolvable-scale diabatic heating or stratiform condensation and therefore requires more realistic model physics to describe the resolvable-scale phase changes (Zhang et al., 1988). Thus, under such a meteorological circumstance, ice microphysics can demonstrate its rôle in reproducing the intensity and distribution of MCSs and associated rainfall. In this model, the resolvable-scale ice-phase microphysics parameterization follows Lin et al. (1983) and Rutledge and Hobbs (1983), and is described briefly in Section 2 and the Appendix. Section 3 provides a sensitivity study of different effects on ice microphysics, such as full ice physics, freezing, melting and sublimation, on the simulation of the Johnstown mesovortex. Section 4 contains a summary and concluding remarks.

2. Model description

The model used for this study is an improved version of the Pennsylvania State University/National Center for Atmospheric Research (PSU/NCAR) mesoscale hydrostatic model originally described by Anthes and Warner (1978); it is very similar to the version used by Zhang and Fritsch (1986a), Zhang et al. (1988) for the same case study of the 1977 Johnstown flood event. The following modifications are considered to be very important for the numerical simulation of mesovortices:

- an *explicit* (i.e., grid-resolved) convective scheme containing predictive equations for cloud water (ice) and rainwater (snow) (Hsie et al., 1984; Lin et al., 1983; Rutledge and Hobbs, 1983); and
- an improved *explicit* (i.e., parameterized) convective scheme of the Fritsch–Chappell (1980, also see Zhang and Fritsch, 1986a) for the fine mesh and the R. A. Anthes–H. L. Kuo (Anthes and Keyser, 1979) for the coarse mesh portion of the nested-grid model.

Other important modifications include a two-way interactive nested-grid procedure (Zhang et al., 1986); a modified version of the Blackadar "large-eddy exchange" planetary boundary layer (PBL) parameterization (Zhang and Anthes, 1982: Zhang and Fritsch, 1986a); and virtual temperature effects in the ideal gas law. The nested-grid ratio is 1 to 3 with a fine-mesh length of 25 km and a coarse-mesh length of 75 km. The number of grid points for the (x, y, σ) dimensions of coarse and fine meshes are $39 \times 31 \times 19$ and $43 \times 37 \times 19$, respectively. The vertical coordinate σ is defined as $\sigma = (p - p_t)/p^*$ and $p^* = p_s - p_t$ where p_t ($=80$ mb) and p_s are the pressure at the top of the model and at the surface, respectively. Since the results from the find mesh domain are of essential interest, the following descriptions will be confined only to the fine-mesh portion of the simulation. All experimental simulations are initialized at 1200 GMT 19 July 1977, and integrated in time for 12 h which is roughly a lifecycle of the Johnstown mesovortex. For a more detailed description of the different model aspects, the reader is referred to Anthes and Warner (1978), Zhang and Fritsch (1986a), Anthes et al. (1987), and Zhang et al. (1988).

The implicit Fritsch–Chappell convective scheme contains individual components of updrafts, moist downdrafts and subgrid compensating subsidence, and includes parameterized freezing and melting effects (see Fritsch and Chappell, 1980). Zhang et al. (1988) and Zhang (1988) showed that the implicit convective scheme is very important for the numerical simulation of convectively driven mesoscale weather systems even with a grid resolution of 12.5 km. Without the Fritsch–Chappell scheme, the explicit convective scheme fails to reproduce any precipitation associated with the squall line system that occurred in the Johnstown flood events, and the mesovortex is overgenerated.

The explicit convective scheme contains the effects of virtual temperature, hydrostatic water loading, condensation and evaporation, freezing and melting, and sublimation. In the present explicit convective scheme, the phase demarcation between liquid water (i.e., cloud water and rainwater) and frozen particles (i.e., cloud ice and snow crystals) is made to be dependent upon the position of a parcel (above or below the 0°C

isotherm). Furthermore, the freezing of cloud water and rainwater, and the melting cloud ice and snow are assumed to occur within a model layer (i.e., about 50 mb thick for this case study) around the 0°C isotherm. Note that the melting of most ice particles generally occurs at one level below the level where the freezing and sublimation become operative due to the discretized nature of the vertical grids, i.e., when $T > 0$°C is checked for melting from the model top downward and $T \leq 0$°C for freezing from the model bottom upward. Supercooled liquid water is not allowed to exist in the model. This is considered to be a reasonable approximation for mesoscale vertical resolution less than 20 layers. The computational advantage of making this approximation is that cloud ice and snow can be stored in the same array as cloud water and rainwater, respectively. The explicit predictive equations for water vapor, q_v, cloud water and ice, q_{wi}, and rainwater and snow, q_{rn}, and the necessary thermodynamic equation are given by:

$$\frac{\partial p^* q_v}{\partial t} = -m^2\left[\frac{\partial(up^* q_v/m)}{\partial x} + \frac{\partial(vp^* q_v/m)}{\partial y}\right] - \frac{\partial p^* q_v \dot{\sigma}}{\partial \sigma} + p^*(P_{ced} + P_{red} - P_{gci}) + p^*(P_{CON} + P_{PBL} + P_{HD} + P_{VD})\, q_v, \quad (1)$$

$$\frac{\partial p^* q_{wi}}{\partial t} = -m^2\left[\frac{\partial(up^* q_{wi}/m)}{\partial x} + \frac{\partial(vp^* q_{wi}/m)}{\partial y}\right] - \frac{\partial p^* q_{wi} \dot{\sigma}}{\partial \sigma} + p^*(P_{gci} - P_{ced} - P_{aut} - P_{acr}) + p^*(F_{PBL} + F_{HD} + F_{VD})\, q_{wi}, \quad (2)$$

$$\frac{\partial p^* q_{rn}}{\partial t} = -m^2\left[\frac{\partial(up^* q_{rn}/m)}{\partial x} + \frac{\partial(vp^* q_{rn}/m)}{\partial y}\right] - \frac{\partial p^* q_{rn} \dot{\sigma}}{\partial \sigma} + p^*(P_{aut} + P_{acr} - P_{red}) - g\frac{\partial(\rho q_{rn} v_t}{\partial s} + p^* F_{HD}\, q_{rn}, \quad (3)$$

$$\frac{\partial p^* T}{\partial t} = -m^2\left[\frac{\partial(up^* T/m)}{\partial x} + \frac{\partial(vp^* T/m)}{\partial y}\right] - \frac{\partial p^* T\dot{\sigma}}{\partial \sigma} + \frac{RT_v w}{C_{pm}(\sigma + p_t/p^*)} + \frac{Lp^*(P_{gci} - P_{ced} - P_{red})}{C_{pm}} - \frac{\delta L_f p^*[\dot{\sigma}(q_{wi} + q_{rn}) + \rho g q_{rn} v_t]}{C_{pm}\,\Delta\sigma} + p^*(F_{CON} + F_{PBL} + F_{HD} + F_{VD})\, T, \quad (4)$$

where

$$\delta = \begin{cases} 1 & \text{at the melting or freezing level,} \\ 0 & \text{at all other levels,} \end{cases} \quad (5)$$

and

$$C_{pm} = C_p(1 + 0.81 q_v) \quad (6)$$

is the specific heat at constant pressure for moist air, and

$$L = \begin{cases} L_v & T > 0\text{°C} \\ L_s = L_v + L_f & T \leq 0\text{°C} \end{cases} \quad (7)$$

where L_v is latent heat of vaporization and L_f is latent heat of fusion, P_{gci} is the initiation rate of cloud water (ice), P_{aut} is the autoconversion rate of cloud droplets (ice crystal) to raindrops (snow), P_{acr} is the accretion rate of cloud droplets (ice crystals) by raindrops (snow), P_{ced} is the evaporation (deposition/sublimation) rate of cloud water (ice), P_{red} is the evaporation (deposition/sublimation) rate of rainwater (snow), and v_t is the mass-weighted mean terminal velocity of raindrops (snow), and F_{CON}, F_{PBL}, F_{HD}, and F_{VD} are the tendency operators for parameterized moist convection, the PBL effect, horizontal diffusion, and vertical diffusion, respectively, and all other variables assume their usual meanings. The term with the parameter δ in eq. (4) denotes the freezing (melting) of liquid water (ice particles) when $\dot{\sigma} < 0$ ($\dot{\sigma} > 0$), and the melting of snow fallouts when they fall through the 0°C isotherm. The specific formulations for the microphysics parameterization in the explicit convective scheme are given in the Appendix.

It should be noted that the implicit and explicit schemes are operating simultaneously in this model to account for the separate effects of

subgrid-scale and mesoscale convection. For the convenience of model description, the explicit convective scheme computes "stratiform" or resolvable-scale precipitation which is generated within a saturated atmosphere (i.e., 100% relative humidity), whereas the implicit convective schemes obtain parameterized convective precipitations which forms in a conditionally unstable and favorably forced but not necessarily saturated environment. As discussed by Zhang et al. (1988), the simultaneous incorporation of implicit and explicit convective schemes (termed "the full physics approach") does not double account for either resolvable-scale or subgrid-scale heating and moistening, since explicit convective schemes neglect subgrid eddy fluxes that implicit convective schemes handle. Zhang et al. (1988) showed that the full physics method appears to be the best approach to handling convective and stratiform precipitation in nature. Although the cloud water (ice) and rainwater (snow) are not explicitly present in the implicit convective schemes, the present approach does not produce any notable discontinuity in the model dynamics and thermodynamics when the model rainfall switches from convective to stratiform mode, or vice versa (see discussion in Zhang et al., 1988). However, the incorporation of cloud water (ice) and rainwater (snow) may affect the profiles of parameterized heating and moistening.

3. Results

There are two types of MCSs involved in the 19–20 July 1977 Johnstown flood events: a convective squall line and a meso-β scale vortex which is embedded in a mesoscale convective complex (MCC, see Maddox, 1980 for its definition). Hoxit et al. (1978), Bosart and Sanders (1981), Zhang and Fritsch (1986a) and Zhang and Fritsch (1987) provided a detailed description for the case study of the Johnstown MCSs. Since the squall line produced little resolvable-scale condensation/precipitation and since implicit convective heating has a much less important effect on the development of the mesovortex than resolvable-scale heating, only the mesovortex and associated resolvable-scale diabatic heating will be emphasized in this paper.

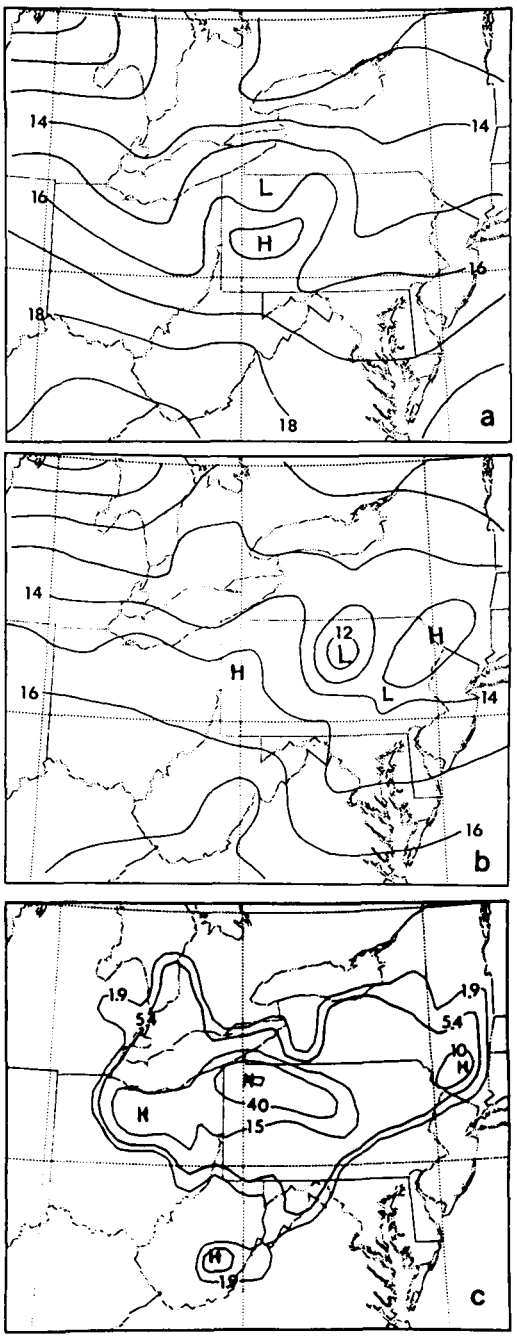

Fig. 1. Analysis of sea-level pressure (mb) from Exp. CTR (control simulation without ice microphysics) for (a) 1800 GMT and (b) 0000 GMT. (c) Predicted 12 h accumulated total rainfall (mm) for the period 1200 GMT 19 to 000 GMT 20 July 1977.

As shown in Zhang and Fritsch (1986b, 1987), the Johnstown mesovortex initiates from a nearly saturated and moist adiabatic environment over Lake Erie in combination with a centralized lifting from a midtropospheric meso-α scale short wave near the model initial time (i.e., 1200 GMT 19 July 1977). As it propagates east-southeastward towards central Pennsylvania, it quickly intensifies with a mesolow pressure extended from the midtroposphere down to the surface around 0000 GMT 20 July (see Figs. 15–18 in Zhang and Fritsch, 1986a and Fig. 1 in Zhang and Fritsch, 1987). The vortex at the mature stage exhibits a closed cyclonic wind circulation in the low- to midtroposphere and an anticyclonic outflow near the tropopause. Its maximum vorticity occurs between 850 and 700 mb. The thermal structure of the vortex is characterized by a pool of cool moist downdraft air from the surface to 850 mb beneath its midtropospheric warm core, and a cold dome in the vicinity of the tropopause above the warm core. The warm-core structure results from the surplus of latent heat release over the adiabatic cooling and horizontal energy dispersion and is responsible for the initial concentration of cyclonic vorticity through the geostrophic adjustment processes. In the decaying stage, the warm-core vortex is primarily maintained by inertial stability of the cyclonic circulation. The vortex drops a significant amount of stratiform rainfall along its path (Zhang and Fritsch, 1987). The observed 12 h local maximum rainfall over northwestern Pennsylvania is more than 100 mm (see Hoxit et al., 1978; Zhang and Fritsch, 1986a).

Although Zhang and Fritsch (1986a) reproduced extremely well the development and evolution of the mesovortex and associated convective weather systems, its strength and associated rainfall amount were overpredicted due to the relatively poor control of the CISK-like instability. Later, by incorporating hydrostatic water loading and evaporative cooling, Zhang et al. (1988) significantly improved the simulation of the vortex strength, accumulated rainfall and associated MCSs, as compared with the observational analyses of Hoxit et al. (1978) and Bosart and Sanders (1981). In the next subsection, this simulation (see Fig. 1) will be utilized as a control run (Exp. CTR) for the purpose of investigating the rôle of ice-phase microphysics in the simulation of the Johnstown mesovortex. Then, in subsection 3.2, individual effects of the parameterized ice microphysics will be examined.

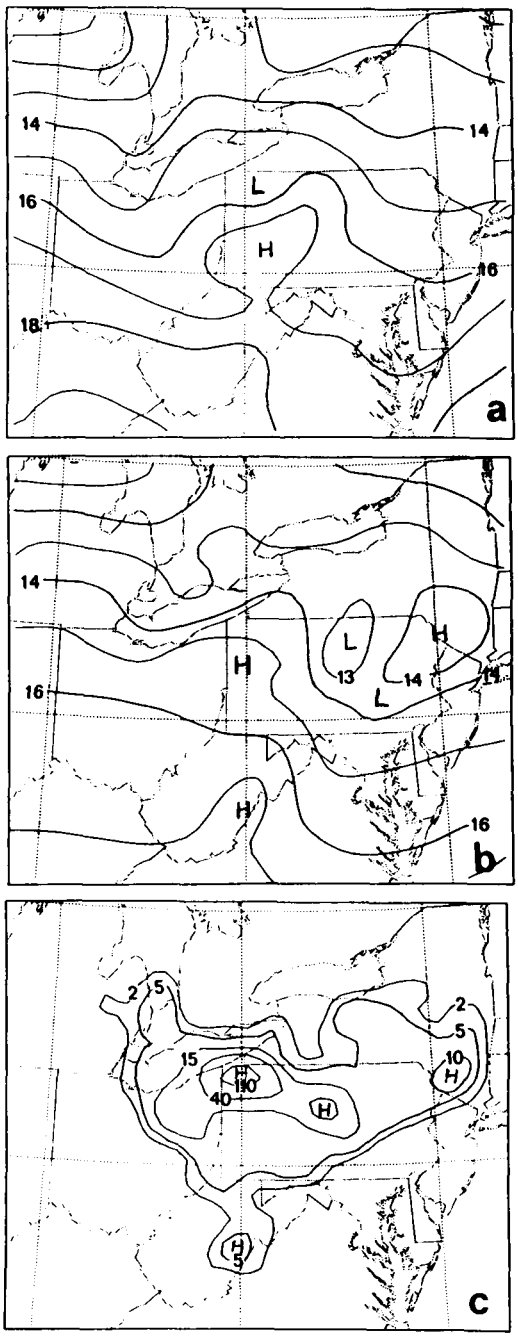

Fig. 2. As in Fig. 1 but for Exp. ICE (with full ice microphysics).

3.1. The effect of full ice microphysics

By incorporating ice microphysics into the explicit convective scheme used for Exp. CTR (Exp. ICE, see Fig. 2), the vortex-related sea-level pressure perturbation at 1800 GMT becomes less significant and the major mesolow at 0000 GMT is about 1 mb weaker than that in Exp. CTR (cf. Figs. 1b and 2b, and see Table 1). Note that since the distribution of model convection and associated temperature perturbation produced by the Fritsch–Chappell implicit convective scheme for all experimental simulations presented here are similar to that in Exp. CTR or in Zhang and Fritsch (1986a), only the domain-accumulated convective rainfall is given in Table 1 for the purpose of the intercomparisons. The appearance of a weak pressure perturbation during the development stage and a closed mesolow at the decaying stage is a characteristic feature of many midlatitude mesovortices (Hoxit et al., 1978; Zhang and Fritsch, 1986a; Rockwood et al., 1984; Johnson, 1986), and can be explained hydrostatically by the well-developed mid-tropospheric warm-core (or high-θ_e core) structure of the cyclonic circulation (see Figs. 7–10 and 11 in Zhang and Fritsch, 1987). Thus, the weaker mesolow in Exp. ICE implies that the cooling due to melting of ice particles compensated for freezing and sublimination effects, and reduced the mean temperatures in the air column beneath the 0°C isotherm. Numerous studies indicate that decreases in the magnitude of the resolvable-scale heating below 500 mb can have a prominent effect on retarding the development of model cyclones (Anthes and Keyser, 1979; Gyakum, 1983; Sardie and Warner, 1983). Hence, the melting may be an important factor in weakening the mesovortex, and this will be examined in the next subsection.

Another important effect of including ice microphysics is related to the timing of initiating the resolvable-scale condensation/precipitation. Fig. 3 shows that with the inclusion of ice microphysics, precipitation begins to develop and reaches its maximum rate nearly one hour earlier. As pointed out by Zhang et al. (1988), there is a common problem in the generation of resolvable-scale condensation for meso- and larger-scale models, namely, an unrealistic delay in the start of the grid-box saturation. Although the control simulation exhibits little delay of the grid-scale condensation and rainfall conversion because of the initial near-saturated environment over Lake Erie, the extent and the number of grid boxes in which the condensation occurs during the initial two model hours are much less than that in Exp. ICE. Thus, the result appears to indicate that *the delay of the resolvable-scale condensate production in meso- or larger-scale numerical weather prediction models could be improved by incorporating realistic ice microphysics into the model.* Moreover, the earlier triggering of the grid-scale condensation and additional latent heat release of fusion appear to have helped accelerate the positive feedback process among latent heat release, low-level moisture convergence and the surface pressure fall

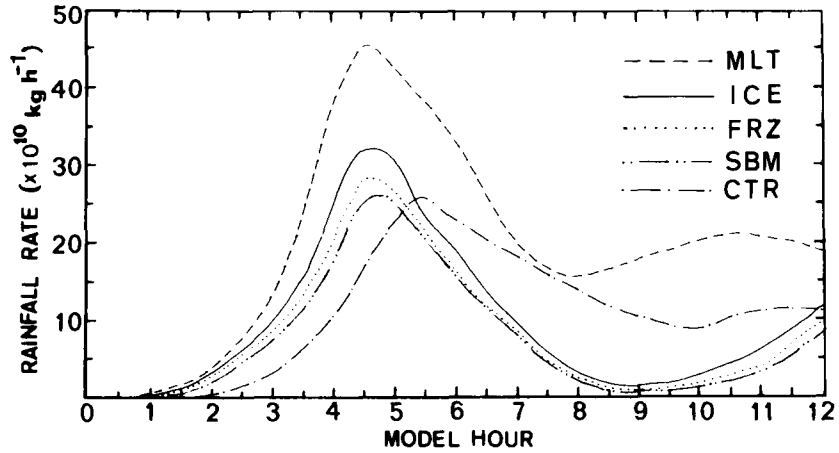

Fig. 3. The predicted hourly domain-integrated resolvable-scale rainfall rate (kg h^{-1}) for individual experimental simulations.

Table 1. *Predicted 12-h domain-accumulated total rainfall volume of convective (R_{con}), resolvable-scale (R_{rs}) and local maximum (R_H); minimum sea-level pressure (P_L) pf the mesolow and local maximum vertical motion ($-\omega_H$) for individual experimental simulations*

Code	Description of simulations	R_{con} (10^{12} kg)	R_{rs} (10^{12} kg)	R_H (mm)	P_L (mb)	$-\omega_H$ (μb s^{-1})
CTR	no ice control	2.76	1.41	117	1011.4	215
a: ICE	full ice microphysics	2.36	1.18	140	1012.3	243
b: MLT	no melting	2.41	2.42	202	1007.5	324
c: FRZ	no freezing	2.26	1.03	124	1012.8	198
d: SBM	no sublimation	2.24	0.94	118	1013.0	185

that is responsible for the initial rapid development of the mesovortex. As a consequence, the local maximum upward motion ($-\omega$) and accumulated rainfall in Exp. ICE are significantly larger than that in Exp. CTR (see Table 1). Notice that the rainfall rate in Exp. ICE quickly decreases after the sixth model hour. As will be shown in the next subsection, this can be attributed to the dominant rôle of melting in retarding the preceding-mentioned positive feedback process. Of particular interest is that although the hourly resolvable-scale rainfall rate during first 5.5 h (Fig. 3) and the maximum locally accumulated rainfall over northwestern Pennsylvania (Table 1) in Exp. ICE are much larger than that in Exp. CTR, the surface pressure perturbation at 1800 GMT is not as significant as that in Exp. CTR. The physical processes involved can be understood as follows. Since the lapse rate of an ice moist adiabat is larger than a liquid moist adiabat due to the additional latent heat release by fusion, an air parcel lifted by the mesoscale ascent within the nearly water-saturated vortex layers (see Fig. 8 in Zhang and Fritsch, 1987) will become less stable or unstable along the ice moist adiabat. This implies that vertical circulation will be enhanced, generally leading to augmented snow crystals or precipitation (cf. Figs. 1c, 2c). However, an increase in precipitable particles tends to not only enhance cooling due to the melting as more snow crystals fall through the 0°C isotherm but also increase the hydrostatic water loading effect, and thus retard the development of strong upward motion and cyclonic vorticity. The former point will be further discussed in the following paragraphs. As a result of a relatively weak mesovortex, the 12 h domain-accumulated rainfall associated with the mesovortex in Exp. ICE is about 20% less than that in Exp. CTR (see Table 1).

In essence, the above-discussed differences can be attributed to the differences in the resolvable-scale heating profile and in the response of the wind field to the perturbed mass field. Fig. 4 shows the pressure–time cross section of the maximum area-averaged (i.e., 9-point average around the vortex center) resolvable-scale diabatic heating rate (DT/Dt, °C h^{-1}), vertical motion ($-$OMG, μb s^{-1}) and relative vorticity (VOR, 10^{-5} s^{-1}) for Exps. ICE and CTR. Note that the hourly resolvable-scale heating rate profiles are obtained from their instantaneous values. The dashed lines denote the time evolution of local maxima in the vertical. Several similarities between the left and right panels are worth mentioning first. For example, the maximum upward motion develops nearly in phase with the diabatic heating both in time and space. The development of the maximum cyclonic vorticity in lower levels and anticyclonic vorticity near the tropopause lags about two hours behind the maximum rate of diabatic heating. The maximum vorticity is also slightly out of phase in space with and to the rear of the maximum upward motion in the low- to mid-troposphere (see Zhang and Fritsch, 1987). The phase shift has also been noted in a numerical simulation of an observed front by Ross and Orlanski (1982). Furthermore, the 2- to 3-h lagging period was found to be an approximate time scale for the wind field to geostrophically adjust to the perturbed mass field in this particular case. Note also that the center of local maximum cyclonic vorticity is displaced downward as the mesovortex spins up as a result of an increase in the resolvable-scale heating rate or low- to mid-level moisture and mass convergence, and vice versa.

The differences produced between these two simulations are of our primarily concern and can be briefly summarized as follows. Firstly, with the inclusion of ice microphysics parameterization, all

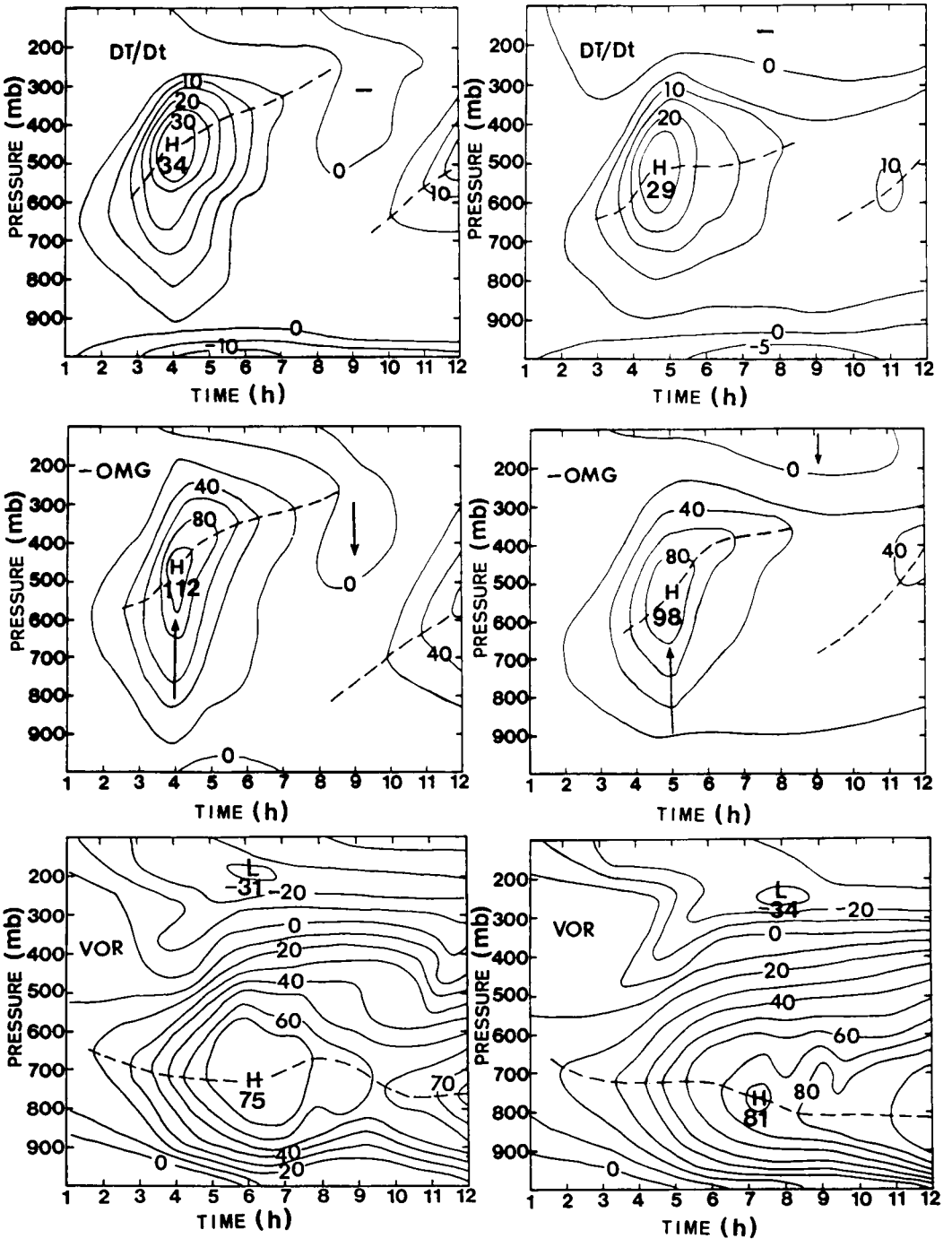

Fig. 4. The pressure–time cross section of the area-averaged (i.e., 9-point around the vortex center) resolvable-scale diabatic heating rate (D*T*/D*t*, °C h^{-1}), vertical motion (−OMG, $\mu b\ s^{-1}$) and relative vorticity (VOR, $10^{-5}\ s^{-1}$). Dashed lines denote the time evolution of local maxima. The left panel is for Exp. ICE (full ice microphysics) and the right panel is for Exp. CTR (control run without ice microphysics).

variables in Fig. 4 reach their maximum values one hour earlier, which is consistent with the evolution of the resolvable-scale rainfall rate. (The maximum rainfall rate lags half an hour behind the maximum diabatic heating). Secondly, the switch from saturation with respect to water to ice increased the maximum heating rate by 5°C h^{-1}, and the maximum upward motion ($-\omega$) by 14 μb s^{-1} whereas it unexpectedly reduced the maximum vorticity by 6×10^{-5} s^{-1}. Moreover, the resolvable-scale rainfall during first six model hours increases considerably (see Fig. 3), but the surface pressure perturbation is less significant, as mentioned before. Thirdly and most importantly, the maximum values of all variables in Fig. 4 for Exp. ICE are shifted upward by more than 50 mb. As is well known, model cyclogenesis is very sensitive to the vertical location of the maximum heating (see Anthes and Keyser, 1979; Gyakum, 1983; Sardie and Warner, 1983; Zhang et al., 1988). Thus, such an upward shifting may be the major reason for why a relatively weak mesovortex but stronger upward motion and more locally accumulated rainfall develop in Exp. ICE. This result tends to suggest that *the vertical distribution of the diabatic heating may be more important than the total amount of heating (i.e., rainfall reaching the ground) in determining the strength of mesovortices* (also see Fig. 3). Fourthly, all variables in Fig. 4 for Exp. ICE tend to decay faster than that in Exp. CTR after reached their maximum values, as can also be seen from Fig. 3. This may reflect the importance of the melting in reducing the net convergence of high-θ_e air through dumping substantial amount of colder air mass into lower troposphere, thereby retarding the above-mentioned positive feedback process. In particular, the melting results in a near discontinuity in the diabatic heating profile around 600 mb where the 0°C isotherm is rougly located. The cooling rate is as large as 5°C h^{-1} within a 50 mb layer depth. This is in agreement with the diagnostic calculation of cooling rate due to the melting effect by Leary and Houze (1979).

3.2. The effects of melting, freezing and sublimation

To gain more insight into individual effects of the ice-phase microphysics on the simulation of the Johnstown mesovortex, three additional experimental simulations are performed by suppressing certain aspects of the diabatic heating in eq. (4) while holding all other conditions the same as Exp. ICE. For these three experimental simulations, the total rainfall distributions will not be shown in Figs. 5–7 since it is similar to that in Exp. ICE or Exp. CTR except for the magnitude of the resolvable-scale and parameterized convective rainfall which has been given in Table 1 and Fig. 3.

When the melting of frozen particles and snow fallouts (Exp. MLT) was neglected from Exp. ICE, the strength of the mesovortex and associated rainfall were unrealistically too intense (see Fig. 5). Specifically, Table 1 shows that the minimum central pressure of the predicted mesolow is 4.7 mb deeper and the 12 h accumulated resolvable-scale rainfall more than doubles that in Exp. ICE. In addition, Fig. 3 displays a more rapid acceleration

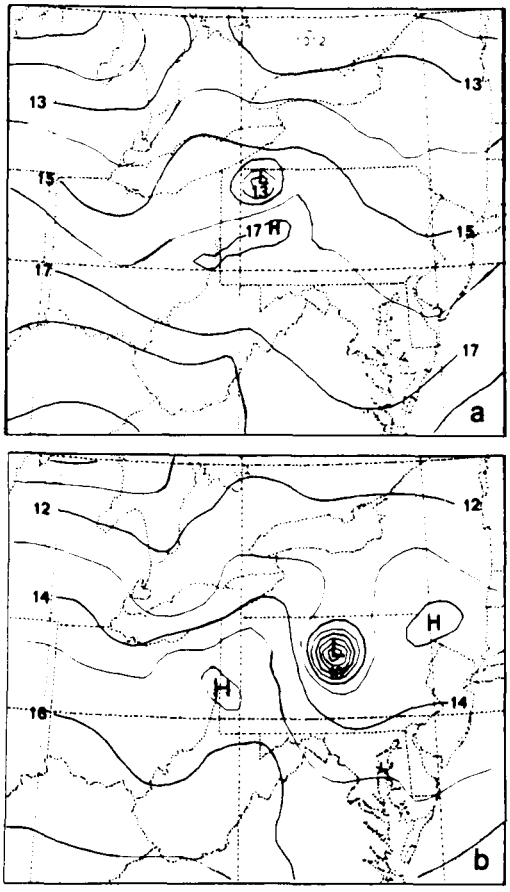

Fig. 5. As in Figs. 1a and 1b but for Exp. MLT (no melting effect).

of the resolvable-scale precipitation during first five model hours and a slower decay thereafter than that in Exp. ICE. As shown in Zhang et al. (1988), liquid water evaporation has little effect on the control of the CISK-like instability before 1800 GMT due to the development of the mesovortex in the nearly saturated environment. Thus, it appears that under nearly saturated conditions, melting can play a much more important rôle than the evaporative cooling in retarding the CISK-like instability and the intensification of the mesovortex. Furthermore, when comparing Exp. MLT with the experimental simulations presented in Zhang et al. (1988) for the same Johnstown MCSs, the neglect of the melting effect is as significant as the omission of hydrostatic water loading and liquid water evaporation in controlling the intensity of mesovortices. It is evident that the significant differences between Exps. ICE and MLT result from the difference in the lower tropospheric heating profile to which numerical models are most sensitive.

When the liquid water is not allowed to freeze as it is advected through the 0°C isotherm by mesoscale ascent (Exp. FRZ), the model produced a mesovortex of the surface pressure 0.5 mb weaker than that in Exp. ICE and 1.4 mb weaker than that in Exp. CTR (see Fig. 6 and Table 1). The local strongest upward motion is also weaker. Nevertheless, the maximum locally accumulated rainfall is still larger than that in Exp. CTR, further suggesting that the magnitude of the resolvable-scale rainfall is not necessarily a good indicator for the intensity of mesovortices if the melting effect is included in a numerical model. The lower model's sensitivity to the freezing than the melting is more likely due to (1) the presence of significant cooling below the 0°C isotherm; (2) the occurrence of the freezing one level above the melting in the model; and (3) the larger amount of ice particles available for melting than liquid water for freezing (i.e., certain amount of rainfall is generated above the 0°C isotherm without going through the freezing process). In addition, the lower-level drying and upper-level moistening by the parameterized convection tend to further enhance the effect of melting and reduce the effect of freezing.

By turning off the fusion of sublimation effect (Exp. SBM) from Exp. ICE, namely, let $L = L_v$ in eq. (4) for $T \leq 0°C$, the model produced the

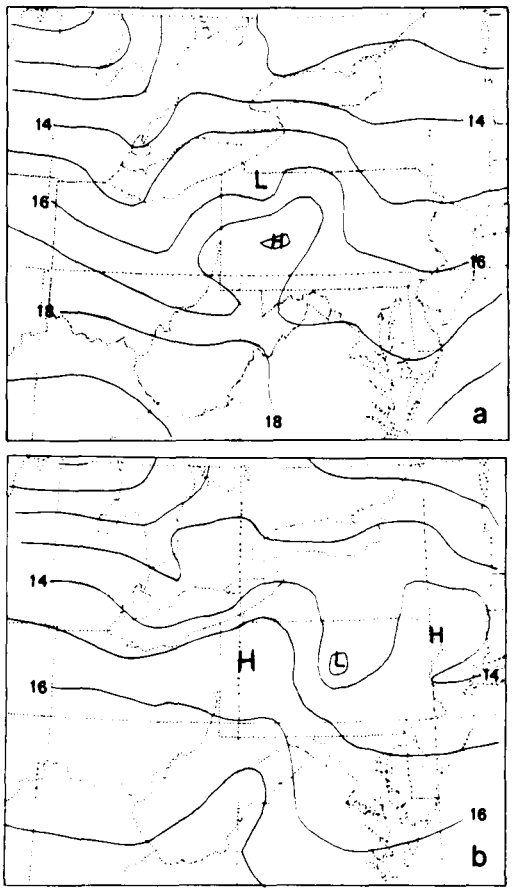

Fig. 6. As in Figs. 1a and 1b but for Exp. FRZ (no freezing effect).

weakest mesovortex (see Fig. 7) as well as the weakest upward motion and resolvable-scale rainfall amount of all the experimental simulations of the Johnstown mesovortex that shown in Table 1 and in Zhang et al. (1988). When comparing Exp. SBM to Exp. FRZ, the model seems to be more sensitive to the sublimation than the freezing in helping spin up the mesovortex. It appears that for this simulation, the melting of ice particles dominates the freezing effect in controlling the strength of the mesovortex due to the same reasons as that stated in the previous paragraph.

Finally, it should be mentioned that the changes in the resolvable-scale ice-phase microphysics produced much smaller variations in the domain-accumulated convective rainfall than that in the resolvable-scale counterpart (see Table 1), and

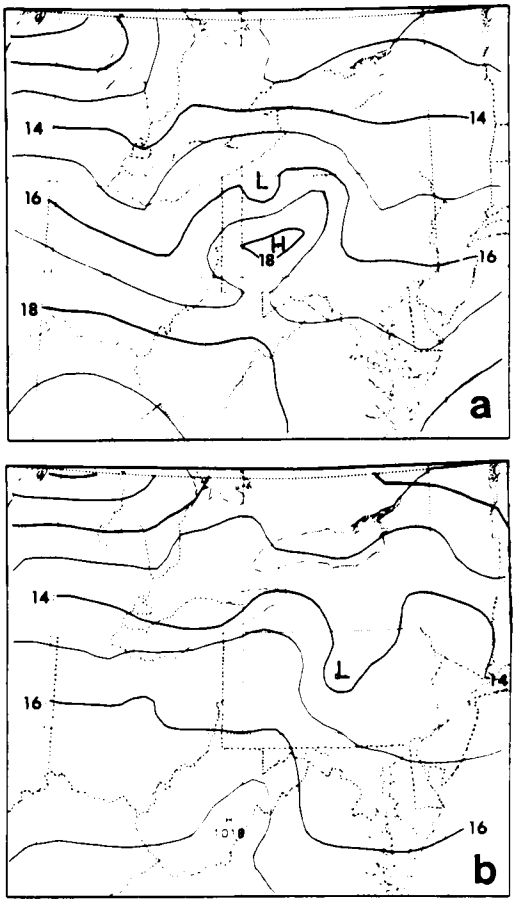

Fig. 7. As in Figs. 1a and 1b but for Exp. SBM (no sublimation effect).

that the time evolution of the convective rainfall for Exps. ICE, MLT, FRZ and SBM (not shown) resembles that for Exp. CTR (see Fig. 3 in Zhang et al., 1988). Thus, the parameterized convection, to certain extent, plays a similar rôle in the generation of the vortex circulation for all experimental simulations and the resolvable-scale or mesoscale convection basically controls the structure and evolution of the Johnstown mesovortex. In fact, Zhang (1988) showed that without the explicit convective scheme, the parameterized convection (produced either by the Fritsch–Chappell or by the Anthes–Kuo scheme) fails to simulate the genesis of the Johnstown mesovortex and associated rainfall. It appears that the generation of the mesovortex/mesolow requires a heating maximum located at relatively lower levels, and *all implicit convective schemes tend to produce the heating maximum at higher levels than explicit condensation would generate.*

4. Summary and concluding remarks

An ice-phase microphysics parameterization has been incorporated into the explicit convective scheme in the PSU/NCAR mesoscale hydrostatic model and tested using the 1977 Johnstown MCSs case with a grid resolution of 25 km. It is found that with the inclusion of ice microphysics parameterization, the resolvable-scale precipitation begins to develop nearly one hour earlier and undergoes a more rapid acceleration. The resulting maximum upward motion and locally accumulated rainfall are significantly larger than that without the ice microphysics. Nevertheless, the model predicted a relatively weak mesovortex with the maximum cyclonic vorticity located more than 50 mb higher when the ice microphysics is included. Sensitivity experiments performed show that the model is most sensitive to the melting, the sublimation and the freezing, in that order. It appears that the combined effects of freezing and sublimation are responsible for the rapid development of the midtropospheric vortex circulation while the melting effect tends to destroy the concentration of lower-tropospheric cyclonic vorticity through stabilizing lower tropospheric column.

Although there is little evidence of resolvable-scale downdrafts due to the melting of ice particles as compared to other studies, it is found that the melting effect can play a rôle as significant as the hydrostatic water loading and evaporative cooling in retarding the development of the CISK-like instability and in reducing the intensity of the mesovortex circulation. In particular, the melting can be more important than the evaporative cooling in destroying the concentration of cyclonic vorticity in nearly saturated conditions. Even though the combined heating by freezing and sublimation generally exceeds the cooling by melting during the development stage, the latter can possibly dominate the former in controlling the strength of the mesovortex. This is because the resulting resolvable-scale heating maximum is shifted upward through the reduction of the lower

tropospheric heating, tending to slow the development of the mesovortex. Thus, the vertical distribution of diabatic heating may be more important than the total heating in determining the intensity of mesovortices when the melting effect is included in a numerical model.

It is important to point out that the significance of the parameterized ice microphysics presented here may be dependent upon the meteorological environmental conditions in which MCSs are embedded. In particular, when MCSs being studied develop under cold-season conditions or in polar regions, the melting of ice particles may have little effect on the lower-level heating profile, and the sublimation effect may dominate the ice microphysics process. It should also be noted that in nature, supercooled liquid droplets and ice crystals generally co-exist in a mixed cloud and freezing occurs well above the 0°C isotherm. In this case, the heating maximum would be shifted further upward, possibly helping weaken the mesovortex further.

5. Acknowledgments

The author is very grateful to J. Dudhia of the Pennsylvania State University for providing the basic coding of the ice-phase microphysics parameterization for this study and to M. W. Moncrieff, Y.-H. Kuo, A. Heymsfield, J. Dudhia and W. D. Hall for their helpful comments. This research was supported by the Advanced Study Program and the Mesoscale and Microscale Meteorology Division, National Center for Atmospheric Research (NCAR) which is sponsored by the National Science Foundation. The Computations were performed on the NCAR CRAY X-MP.

6. Appendix. Cloud microphysics parameterization

The microphysics treatment of the source and sink terms in eqs. (1)–(4) follows Hsie et al. (1984), Lin et al. (1983) and Rutledge and Hobbs (1983). Since the above cited references have provided detailed descriptions of the microphysics treatment, only basic formulations used in the explicit convective scheme will be presented in this appendix for the sake of the model completeness. The reader is referred to original papers for their physical explanations, definitions of symbols and other pertinent information.

A.1. Generation of cloud water and ice (P_{gci})

When $T > 0°C$ and water vapor is supersaturated with respect to water, the condensation rate of water vapor into cloud water is diagnostically computed using

$$P_{gci} = \begin{cases} \dfrac{(q_v - q_{vs})/\Delta t}{1 + L_v^2 q_{vs}/C_{pm} R_v T^2} & q_v > q_{vs} \\ 0 & q_v \le q_{vs}, \end{cases} \tag{A1}$$

where q_{vs} is the saturation specific humidity with respect to water (or ice). Whenever $T \le 0°C$ and the air is supersaturated with respect to ice, the initiation rate of cloud ice from water vapor is given by

$$P_{gci} = \min \begin{cases} (M_o n_c/\rho)/\Delta t \\ (q_v - q_{vs})/\Delta t, \end{cases} \tag{A1'}$$

and it is always

$$P_{gci} \ge 0,$$

where M_o is the initial mass of cloud ice crystals, and n_c is the number concentration of cloud ice crystals which is assumed to be dependent on temperature (Fletcher, 1962):

$$n_c = n_0 \exp [\beta(T_0 - T)]. \tag{A1''}$$

A.2. Autoconversion of cloud water to rainwater and ice to snow (P_{aut})

The autoconversion process is obtained from

$$P_{aut} = \begin{cases} k_1(q_{wi} = q_{w0}) & T > 0°C \\ (q_{wi} - q_{i0})/\Delta t & T \le 0°C, \end{cases} \tag{A2}$$

and it is always

$$P_{aut} \ge 0,$$

where q_{w0} and q_{i0} are critical values for the onset of autoconversion of cloud water to rainwater and cloud ice to snow, respectively, and equal to the respective values of 0.5 g kg^{-1} and $M_{max} n_c/\rho$.

A.3. Evaporation of cloud water and depositional growth of cloud ice (P_{ced})

Below the level of 0°C, whenever the air is subsaturated and cloud water is available, the evaporation rate of cloud water is computed using

$$P_{\text{ced}} = \min \begin{cases} \dfrac{(q_{\text{vs}} - q_{\text{v}})/\Delta t}{1 + L_{\text{v}}^2 q_{\text{vs}}/C_{\text{pm}} R_{\text{v}} T^2} \\ q_{\text{wi}}/\Delta t \end{cases} . \tag{A3}$$

Above the level of 0°C, the sublimation rate of cloud ice and vapor deposition rate onto ice crystals in respective sub- and super-saturated conditions (w.r.t. ice) are given by

$$P_{\text{ced}} = \min \begin{cases} \dfrac{65.2(1 - \text{RH})\,(\rho q_{\text{wi}}\, n_{\text{c}})^{1/2}}{\rho(L_{\text{s}}^2/K_{\text{a}} R_{\text{v}} T^2 + 1/\rho q_{\text{vs}} D_{\text{f}})} \\ (q_{\text{ve}} - q_{\text{v}})/\Delta t) \end{cases} \tag{A3'}$$

where RH, K_{a} and D_{f} are the relative humidity, thermal conductivity of air and diffusivity of water vapor, respectively. Note that $P_{\text{ced}} = 0$ when available water vapor (i.e., $q_{\text{v}} - q_{\text{vs}}$) has been used up by the ice generation process.

A.4. Evaporation of rainwater and depositional growth of snow (P_{red})

When the air is subsaturated with respect to water surface, the evaporation rate of raindrops below the 0°C isotherm is given by

$$P_{\text{red}} = \min \begin{cases} \dfrac{2\pi(1 - \text{RH})\, n_{\text{w}} \left[0.78\lambda_{\text{w}}^{-2} + 0.32 S_{\text{c}}^{1/8} \right.}{\left. \times \Gamma\left(\dfrac{b_{\text{w}} + 5}{2}\right) (a_{\text{w}}/\eta)^{1/2}\, \lambda_{\text{w}}^{-(b_{\text{s}} + 5/2)} \right]} \\ \rho\left(\dfrac{L_{\text{w}}^2}{K_{\text{a}} R_{\text{v}} T^2} + \dfrac{1}{\rho q_{\text{vw}} D_{\text{f}}}\right) \\ q_{\text{rn}}/\Delta t \end{cases} , \tag{A4}$$

where λ_{w} is the slope of raindrop size distribution, S_{c} the Schmidt number (η/D_{f}) and η kinetic viscosity of air. When the air is supersaturated with respect to ice above the 0°C isotherm, snow crystals will grow at the expense of water vapor, but sublimate into water vapor when subsaturated with respect to ice. These processes are computed by

$$P_{\text{red}} = \min \begin{cases} \dfrac{2\pi(1 - \text{RH})\, n_{\text{s}} \left[0.78\lambda_{\text{s}}^{-2} + 0.32 S_{\text{c}}^{1/8} \right.}{\left. \times \Gamma\left(\dfrac{b_{\text{s}} + 5}{2}\right) (a_{\text{s}}/\eta)^{1/2}\, \lambda_{\text{s}}^{-(b_{\text{s}} + 5/2)} \right]} \\ \rho\left(\dfrac{L_{\text{s}}^2}{K_{\text{a}} R_{\text{v}} T^2} + \dfrac{1}{\rho q_{\text{vs}} D_{\text{f}}}\right) \\ q_{\text{rn}}/\Delta t \end{cases} , \tag{A4'}$$

where λ_{s} is the slope of snow size distribution. Note also that $P_{\text{red}} = 0$ when available moisture has all been used up by the ice generation and depositional ice growth processes (i.e., $(q_{\text{v}} - q_{\text{vs}}) \le (P_{\text{gci}} + P_{\text{ced}})\,\Delta t$). That is, the priority transferring available moisture into frozen particles in the model is given to ice generation, deposition onto cloud ice and onto snow, in that order.

A.5. Accretion of cloud water by raindrops and ice crystals by snow (P_{acr})

Below the level of $T = 0$°C, the collection of cloud water by rainwater in the vertical is given by

$$P_{\text{acr}} = \begin{cases} \dfrac{\pi E_{\text{w}}\, n_{\text{w}}\, a_{\text{w}}\, \Gamma(3 + b_{\text{w}})\, q_{\text{wi}}}{4\lambda_{\text{w}}^{3 + b_{\text{w}}}} & q_{\text{rn}} > 0 \\ 0 & q_{\text{rn}} \le 0, \end{cases} \tag{A5}$$

where E_{w} is the collection efficiency for raindrops. The collection of cloud ice by snow is given by

$$P_{\text{acr}} = \begin{cases} \dfrac{\pi E_{\text{s}}\, n_{\text{s}}\, a_{\text{s}}\, \Gamma(3 + b_{\text{s}})\, q_{\text{wi}}}{4\lambda_{\text{s}}^{3 + b_{\text{s}}}} & q_{\text{rn}} > 0 \\ 0 & q_{\text{rn}} \le 0, \end{cases} \tag{A5'}$$

where E_{s} is the collection efficiency for snow. Note that the accretion of cloud water by snow is not considered.

A.6. Terminal velocity of raindrops and snow (v_t)

All precipitable particles are assumed to fall at their mass-weighted terminal velocity. For raindrops, v_{t} is computed according to

$$v_{\text{t}} = \frac{a_{\text{w}}\, \Gamma(4 + b_{\text{w}})}{6}\, \lambda_{\text{w}}^{-b_{\text{w}}} \left(\frac{p_0}{p}\right)^{0.4} . \tag{A6}$$

For snow, it is

$$v_{\text{t}} = \frac{a_{\text{w}}\, \Gamma(4 + b_{\text{w}})}{6}\, \lambda_{\text{w}}^{-b_{\text{w}}} \left(\frac{p_0}{p}\right)^{0.4} . \tag{A6}$$

The factor $(p_0/p)^{0.4}$ accounts for the change in fallspeed with altitude. Note that eqs. (A6) and (A6′) are adapted from meso-γ scale cloud models using grid resolution much less than 5 km (e.g., Lin et al., 1983). When they are applied to meso-β or larger scale models, the resulting fallspeed may sometimes be too large to account for the hydrostatic water loading effect in nature because of the relative weak resolvable-scale vertical motion in comparison with that in high-resolution cloud models. Thus, the grid resolution effect on the resolvable-scale vertical motion may need to be incorporated into the above formulations when a

numerical models tends to overproduce or falsely predict the occurrence of mesocyclogeneses. Zhang et al. (1988), Molinari and Dudek (1986) and Orville et al. (1975) have showed that numerical simulations of MCSs are very sensitive to the water loading effect.

It should be pointed out that to insure the mass conservation of water vapor, cloud water (ice) and rainwater (snow) in calculating the above production terms, some special measures have to be taken. For example, when computing the condensation (evaporation) rate, temperature and water vapor (cloud water or rainwater) are forecast first to see how much water vapor (cloud water or rainwater) is available. The related tendencies used for such forecasts include all possible updated physical processes except numerical diffusions. Note that the diffusions are used to update individual variables when all production terms in eqs. (1)–(4) have been obtained. Similar procedures apply to vapor, cloud ice and snow for their associated computations. Furthermore, the production terms of autoconversion, accretion, evaporation (sublimation) and initiation of cloud water (ice) have to be adjusted when the need for the production $(P_{aut} + P_{acr} + P_{ced} + P_{gci})\,\Delta t$ in eq. (2) exceeds the available amount of q_{wi}.

REFERENCES

Anthes, R. A. and Warner, T. T. 1978. The development of mesoscale models suitable for air pollution and other meteorological studies. *Mon. Wea. Rev. 106*, 1045–1078.

Anthes, R. A., Hsie, E.-Y. and Kuo, Y.-H. 1987 . Description of the Penn State/NCAR mesoscale model version 4 (MM4). *NCAR Tech. Note, NCAR/TN-282*, 66 pp.

Anthes, R. A. and Keyser, D. 1979. Tests of a fine-mesh model over Europe and the United States. *Mon. Wea. Rev. 107*, 963–984.

Bergeron, T. 1935. On the physics of cloud and precipitation. *Proc. 5th Assembly IUGG*, Lisbon, 156–178.

Bosart, L. R. and Sanders, F. 1981. The Johnstown flood of July 1977: A long-lived convective storm. *J. Atmos. Sci. 38*, 1616–1642.

Brown, J. M. 1979. Mesoscale unsaturated downdraft driven by rainfall evaporation: A numerical study. *J. Atmos. Sci. 36*, 313–338.

Chong, M., Amayenc, P., Scialom, G. and Testud, J. 1987. A tropical squall line observed during the COPT 81 experiment in West Africal Part I: Kinematic structure inferred from dual-Doppler radar data. *Mon. Wea. Rev. 115*, 670–694.

Churchill, D. D. and Houze, R. A., Jr. 1984. Development and structure of winter monsoon cloud clusters on 10 December 1978. *J. Atmos. Sci. 41*, 933–960.

Cotton, W. R., Stephens, M. A., Nehrkorn, T. and Tripoli, G. J. 1982. The Colorado State University three-dimensional cloud/mesoscale model–1982. Part II: An ice phase parameterization. *J. Rech. Atmos. 16*, 295–320.

Fletcher, N. H. 1962. *The physics of rainclouds*. Cambridge: Univ. Press, 386 pp.

Fritsch, J. M. and Chappell, C. F. 1980. Numerical prediction of convectively driven mesoscale pressure systems. Part I : Convective parameterization. *J. Atmos. Sci. 37*, 1722–1733.

Gyakum, J. R. 1983. On the evolution of the QE-II storm. II: Dynamic and thermodynamic structure. *Mon. Wea. Rev. 111*, 1156–1173.

Hoxit, L. R., Maddox, R. A., Chappell, C. F., Zuckerberg, F. L., Mogil, H. M., Jones, I., Greene, D. R., Saffle, R. E. and Scofield, R. A. 1978. Meteorological analysis of the Johnstown, Pennsylvania, flash flood, 19–20 July 1977. *NOAA Tech. Rep. ERL 401-APCL43*, 71 pp.

Hsie, E.-Y., Anthes, R. A. and Keyser, D. 1984. Numerical simulation of frontogenesis in a moist atmosphere. *J. Atmos. Sci. 41*, 2581–2594.

Houze, R. A., Jr. 1977. Structure and dynamics of a tropical squall-line system. *Mon. Wea. Rev. 105*, 1540–1567.

Johnson, R. H. 1986. The development of organized mesoscale circulations within Oklahoma-Kansas PreSTORM convective systems. *Preprints, Inter. Conf. on Monsoon and Mesoscale Meteor.*, Taiwan, 100–104.

Kalb, M. W. 1987. The role of convective parameterization in the simulation of a Gulf coast precipitation system. *Mon. Wea. Rev. 115*, 214–234.

Kasahara, A. 1961. A numerical experiment on the development of a tropical cyclone. *J. Meteor. 18*, 259–282.

Leary, C. A. 1980. Temperature and humidity profiles in mesoscale unsaturated downdrafts. *J. Atmos. Sci. 37*, 1005–1012.

Leary, C. A. and Houze, R. A., Jr. 1979. Melting and evaporation of hydrometers in precipitation from anvil clouds of deep tropical convection. *J. Atmos. Sci. 36*, 669–679.

Leary, C. A. and Rappaport, E. N. 1987. The life cycle and internal structure of a mesoscale convective complex. *Mon. Wea. Rev. 115*, 1503–1527.

Lin, Y.-L., Farley, R. D. and Orville, H. D. 1983. Bulk parameterization of the snow field in a cloud model. *J. Climate and Appl. Meteor. 22*, 1065–1092.

Lord, S. J., Willoughby, H. E. and Piotrowicz, J. M.

1984. Role of a parameterized ice-phase microphysics in an axisymmetric, nonhydrostatic tropical cyclone model. *J. Atmos. Sci. 41*, 2836–2848.

Maddox, R. A. 1980. Mesoscale convective complexes. *Bull. Amer. Meteor. Soc. 61*, 1374–1387.

Maddox, R. A. 1983. Large-scale meteorological conditions associated with midlatitude, mesoscale convective complexes. *Mon. Wea. Rev. 111*, 1475–1493.

Molinari, J. and Dudek, M. 1986. Implicit versus explicit convective heating in numerical weather prediction models. *Mon. Wea. Rev. 114*, 1822–1381.

Ogura, Y. and Liou, M.-T. 1980. The structure of a midlatitude squall line: A case study. *J. Atmos. Sci. 37*, 553–567.

Orville, H. D., Kopp, F. J. and Myers, C. G. 1975. The dynamics and thermodynamics of precipitation loading. *Pure Appl. Geophys. 113*, 983–1004.

Orville, H. D. and Kopp, F. J. 1977. Numerical simulation of the history of a hailstorm. *J. Atmos. Sci. 34*, 1596–1618.

Rockwood, A. A., Bartels, D. L. and Maddox, R. A. 1984. Precipitation characteristics of a dual mesoscale convective complex. *NOAA Tech. Rep. ERL ESG-6*, 50 pp.

Ross, B. B. and Orlanski, I. 1982. The evolution of an observed cold front. Part I: Numerical simulation. *J. Atmos. Sci. 39*, 296–327.

Rutledge, S. A. and Hobbs, P. V. 1983. The mesoscale and microscale structure and organization of clouds and precipitation in midlatitude cyclones. VIII: A model for the "seeder-feeder" process in warm-frontal rainbands. *J. Atmos. Sci. 40*, 1185–1206.

Rutledge, S. A. and Houze, R. A., Jr. 1987. A diagnostic modeling study of the trailing stratiform region of a midlatitude squall line. *J. Atmos. Sci. 44*, 2640–2656.

Sardie, J. M. and Warner, T. T. 1983. On the mechanism for the development of polar lows. *J. Atmos. Sci. 40*, 869–881.

Simpson, J., Simpson, R. H., Andrews, D. A. and Eaton, M. A. 1965. Experimental cumulus dynamics. *Rev. Geophys. 3*, 387–431.

Smull, B. F. and Houze, R. A., Jr. 1987. Dual-Doppler radar analysis of a midlatitude squall line with a trailing region of stratiform rain. *J. Atmos. Sci. 44*, 2128–2148.

Srivastava, R. C. 1987. A model of intense downdrafts driven by the melting and evaporation of precipitation. *J. Atmos. Sci. 44*, 1752–1773.

Willoughby, H. E., Jin, H.-L., Lord, S. J. and Piotrowicz, J. M. 1984. Hurricane structure and evolution as simulated by an axisymmetric, nonhydrostatic numerical model. *J. Atmos. Sci. 41*, 1169–1186.

Zhang, D.-L. and Anthes, R. A. 1982. A high-resolution model of the planetary boundary layer—sensitivity tests and comparisons with SESAME-79 data. *J. Appl. Meteor. 21*, 15943–1609.

Zhang, D.-L., Chang, H.-R., Seaman, N. L., Warner, T. T. and Fritsch, J. M. 1986. A two-way interactive nesting procedure with variable terrain resolution. *Mon. Wea. Rev. 114*, 1330–1339.

Zhang, D.-L. and Fritsch, J. M. 1986a. Numerical simulation of the meso-β scale structure and evolution of the 1977 Johnstown floor. Part I: Model description and verification. *J. Atmos. Sci. 43*, 1913–1943.

Zhang, D.-L. and Fritsch. 1986b. A case study of the sensitivity of the numerical simulation of mesoscale convective systems to varying initial conditions. *Mon. Wea. Rev. 114*, 2418–2431.

Zhang, D.-L. and Fritsch, J. M. 1987. Numerical simulation of the meso-β scale structure and evolution of the 1977 Johnstown flood. Part II: Inertially stable warm-core vortex and the mesoscale convective complex. *J. Atmos. Sci. 44*, 2593–2612.

Zhang, D.-L., Hsie, E.-Y. and Moncrieff, M. W. 1988. A comparison of explicit and implicit predictions of convective and stratiform precipitating weather systems with a meso-β scale numerical model. *Quart. J. Roy. Meteor. Soc. 114*, 31–60.

Zhang, D.-L. 1988. The roles of parameterized and grid-resolved convective schemes in the simulation of mesoscale precipitating weather systems. *Preprint, eighth Conf. on Numer. Wea. Prediction*, Amer. Meteor. Soc., 378–383.

Zipser, E. J. 1969. The role of organized unsaturated convective downdrafts in the structure and rapid decay of an equatorial disturbance. *J. Appl. Meteor. 8*, 799–814.

Zipser, E. J. 1977. Mesoscale and convective-scale downdrafts as distinct components of squall-line circulation. *Mon. Wea. Rev. 105*, 1568–1589.